Acta Geotechnica (2018) 13:39–49
https://doi.org/10.1007/s11440-017-0602-9

RESEARCH PAPER

Theoretical analysis of desiccation crack spacing of a thin, long soil layer

Susanga Costa[1] · Jayantha Kodikara[2] · S. L. Barbour[3] · D. G. Fredlund[4]

Received: 1 May 2017 / Accepted: 11 October 2017 / Published online: 15 November 2017

Abstract Soil desiccation cracking is important for a range of engineering applications, but the theoretical advancement of this process is less than satisfactory. In particular, it is not well understood how the crack spacing-to-depth ratio depends on soil material behaviour. In the past, two approaches, namely stress relief and energy balance, have been used to predict the crack spacing-to-depth ratio. The current paper utilises these two approaches to predict the approximate spacing-to-depth ratio of parallel cracks that form in long desiccating soil layers subjected to uniform tensile stress (or suction profile) while resting on a hard base. The theoretical developments have examined the formation of simultaneous and sequential crack patterns and have identified an important relationship between the stress relief and energy approaches. In agreement with experimental observations, it was shown that the spacing-to-depth ratio decreases with layer depth, and crack spacing generally increases with layer depth. The influence of the stiffness at the base interface indicated that decreasing the basal interface stiffness makes the crack spacing to increase in sequential crack formation. The experimental observations also show a decrease in cracking water content with the decrease in layer thickness, and this behaviour was explained on the basis of a critical depth concept.

Keywords Cracking · Desiccation · Fracture toughness · Moisture · Soil · Tensile strength

List of symbols

d	Depth of the clay layer
E	Elastic modulus of clay layer
E_f	Energy consumed by crack formation ($= G_c d$)
E_f^*	Dimensionless form of E_f
G_c	Crack energy release rate
k	Shear stiffness of the interface between clay and hard base
K_{IC}	Fracture toughness in Mode I (pure tensile) cracking
s	Crack spacing
u_b	Relative displacement at the basal interface
x	Distance from the crack face
w_{cr}	Water content at crack initiation
α	Factor of tensile strength needed to from a sequential crack
$\Delta\sigma_x$	Change in normal stress in x direction
$\Delta\varepsilon_x, \Delta\varepsilon_y, \Delta\varepsilon_{xy}$	Change in strain in x and y directions
$\Delta U, \Delta U^*$	Change in strain energy and its dimensionless form
$\sigma_x^{av}, \sigma_y^{av}, \tau_{xy}^{av}$	Average normal stresses and shear stresses in x and y directions
υ	Poisson's ratio
τ_b	Shear stress at the base of the interface
σ_o	Normal stress prior to cracking

✉ Jayantha Kodikara
Jayantha.kodikara@monash.edu

[1] School of Engineering and IT, Federation University Australia, Churchill, VIC, Australia

[2] Department of Civil Engineering, Monash University, Victoria 3800, Australia

[3] Department of Civil, Geological and Environmental Engineering, University of Saskatchewan, Saskatoon, Canada

[4] Golder Associates Ltd, Saskatoon, SK, Canada

σ_t Tensile strength of soil
σ_{xc} Horizontal stress due to an isolated crack subject to uniform compressive stress

1 Introduction

Desiccation cracking can have a severe impact on the performance of clay soils in various geotechnical, agricultural and environmental applications. In geotechnical engineering, the presence of desiccation cracks can weaken the stability, serviceability and hydraulic performance of earthen structures. In agricultural science, cracks can be beneficial for aeration and plant-root growth, but can pose problems as a result of rapid water and solute movement through cracks. In geo-environmental engineering, barriers of low hydraulic conductivity made of compacted and natural clayey soils are commonly relied upon to minimise the contamination of soil and groundwater. The development of desiccation cracks can rapidly deteriorate the performance of low hydraulic conductivity barriers. It follows that in the design of these structures a deeper understanding of crack formation and the development of predictive tools for crack formation could be of great benefit.

Previous studies of desiccation cracking have spread across several disciplines and date back to the early twentieth century [16]. The majority of these studies are predominantly qualitative, highlighting the observations on crack depth and spacing, and the mechanism of crack formation [18]. These studies have shown that crack initiation and propagation are affected by the layer thickness, drying rate, initial moisture content, specimen size, soil type and fracture properties of the material [e.g. 8–11, 21, 23–26]. However, theoretical research on desiccation crack spacing and the relationship of depth-to-spacing ratio is relatively limited, and the current understanding is less than satisfactory. Basically, two approaches have been utilised in the past for examining crack spacing-to-depth ratio in drying or cooling of materials. The first involves the use of stress relief caused by crack formation where the distance between the first crack and second crack is examined [21, 22]. Kodikara and Choi [19] also examined the use of stress relief to predict subdivision that takes place in sequential cracking of clay layers of finite extent. The second approach involves the use of energy balance between the strain energy released and the energy used in formation of new cracks [4]. While these two approaches appear to capture the essential physics influencing crack spacing, the combined influence of stress relief and energy balance is not clear and the prediction of crack spacing in desiccating soil is not possible with any certainty. A rigorous analysis of the problem is unduly complex due to multitude of interacting nonlinear processes. These processes include material property changes (e.g. strength and stiffness) with drying increase in suction and soil stress due to moisture evaporation under ambient climatic conditions, and crack initiation and crack propagation influenced by changing soil behaviour and boundary conditions. A complete theoretical model will need to incorporate the interaction of all the above variables in order to simulate the evolution of cracking patterns. The simulation could only be accomplished through the use of a highly complex numerical model. In the recent past, some researchers [1, 2, 12, 20, 28] attempted to handle this complicated problem by simplified approaches. In addition to the apparent deterministic processes involved, the desiccation cracking process is also dependant on the distribution of micro-cracks within the material and/or spatial variations in the material properties, particularly the tensile strength of the soil. It would be almost impossible to develop a complete model that would predict the exact crack patterns of desiccating soil because of the inherent stochastic nature of the soil. It may, however, be possible to theoretically predict cracking patterns that are statistically similar to the actual behaviour and determine parameters of crack statistics. The development of this capability is beneficial because its application is not only confined to the desiccation of soil but also to a range of other industrial processes, involving the drying of porous materials (e.g. ceramic, polymers and cemented materials). The statistical nature of the cracking process has been explained by some researchers (e.g. [5–7]).

Approximate theoretical formulations are developed for the crack spacing of a desiccating long soil layer resting on a hard base in this paper. The formulations are used to explain some crack behavioural patterns and intriguing observations made on desiccation cracking in the laboratory and the field. The assumption is made that cracks occur under plane conditions (i.e. parallel cracking) in linear elastic materials. Once the crack is initiated, it will propagate to the full depth of the layer. It is assumed that a near uniform shrinkage stress distribution occurs across the layer depth. This is a reasonable assumption for relatively thin clay layers losing moisture [14]. Based upon these assumptions, the work is considered to be relevant for the interpretation of laboratory test data and for field applications involving relatively thin geomaterial layers such as clayey liners and road pavements.

2 Basic mechanisms

Crack initiation is generally modelled using a strength criterion. Under uniaxial conditions, the tensile strength (σ_t) can be simply determined from the tensile stress (σ) generated due to the matric suction at failure (i.e. when $\sigma = \sigma_t$). Tensile stresses within the soil medium are generated when the soil is in some way restrained against potential shrinkage. These restraints can initially come from non-uniform shrinkage and/or at the interfaces between various materials. Generally, cracks initiate at the soil surface where the horizontal tensile stress is the highest. It is also possible to initiate a crack at some depth due to defects, combined stress conditions and the shape of the suction profile. The effect of defects in crack initiation was illustrated by Costa et al. [11]. Once cracks are initiated, the depth of propagation is governed by energy release due to energy consumption for the formation of cracks as characterised by material fracture toughness. Konrad and Ayad [21] used this approach to compute the stable depth of an isolated crack.

The relationship between crack depth and spacing is not clear although there is a general trend of larger crack spacing for deeper cracks as observed from field evidence [9, 11]. As suggested by Costa et al. [11] from the laboratory experiments of circular specimens, shallow, closely spaced cracks are commonly observed on clay surfaces owing to rapid desiccation after a heavy rain. Deeper cracks, widely spaced, are normally associated with slow desiccation. Therefore, it appears that fracture spacing may be strongly related to the depth and intensity of the suction profile developed in the soil. Using a stress relief (or perturbation) approach, the spacing associated with the development of a second crack will depend on the zone of stress relief caused by the first crack. If a crack has already formed, a zone of stress relief is generated where the tensile stress on the surface will be zero at the crack and will increase asymptotically with depth. A second crack is likely to occur when the tensile stress on the surface (where it is considered to be the largest) reaches the tensile strength of the material. Ignoring the change in tensile strength with drying time, some [21, 22] have argued that the second crack occurs sequentially when the developed tensile stress approaches a significant fraction (e.g. 90%) of the tensile strength of the material. This allows an estimate to be made of the likely crack spacing. Ayad et al. [3] applied this concept in the analysis of their field results and indicated that the average spacing in the field could be predicted if the factor was around 80 to 88% of the tensile strength. This factor is somewhat arbitrary, and its relationship to physical behaviour was not explained. In this paper, an explanation is provided for this factor using the fracture mechanics principal.

Several researchers [11, 17, 18] attempted to provide an explanation for possible theoretical patterns and observed field cracking patterns in homogenous media. Theoretically plausible cracking patterns in homogenous media were considered under parallel, orthogonal (square) and non-orthogonal (triangular and hexagonal) patterns. It was found that hexagonal patterns provided the most efficient geometrical shape for energy release during cracking, followed by square and triangular patterns. These theoretical patterns have been observed in experimental and field observations, but combination of these patterns and their variations are also common. The combinations are believed due to spatial variations in material properties, material thickness and drying conditions. Geometric shapes comprising 4 and 5 sides are most common with predominantly orthogonal crack intersections.

Predominantly parallel cracks are common in long strips of material such as the fractures found in road pavements, concrete pathways, and in laboratory tests where the soil is subjected to linear shrinkage [18, 23, 24]. Parallel crack patterns have also been observed parallel to the crest of slopes and between rows of plants such as corn [30]. Parallel cracks are simple in nature and less complicated for analysis purposes. The following sections of this paper present two approaches, namely stress relief approach and energy balance approach, which can be used to predict spacing between parallel cracks.

3 Application of stress relief approach

The stress relief arising from an isolated crack penetrating to the full depth of an elastic clay layer, due to the development of a uniform suction profile, is examined as part of this research programme. The influence of the bottom interface was simulated using a spring of stiffness k, which gives a linear relationship between the bottom shear stress and shear displacement. The method of superposition was used to separate the problem into two parts for the theoretical analysis as shown in Fig. 1. Figure 1a shows the condition after a crack has formed, while Fig. 1b shows uniform conditions prior to the formation of a crack, and Fig. 1c shows the cracked condition with compressive stresses applied on the crack surface. Therefore, the horizontal tensile stress remaining after the crack is formed, σ_x, can be expressed as:

$$\sigma_x = -\sigma_0 + \sigma_{xc} \quad (1)$$

where $(-\sigma_0)$ is the original horizontal tensile stress and σ_{xc} is the horizontal tensile stress (at any general location [x, y]) due to an isolated crack subjected to a uniform

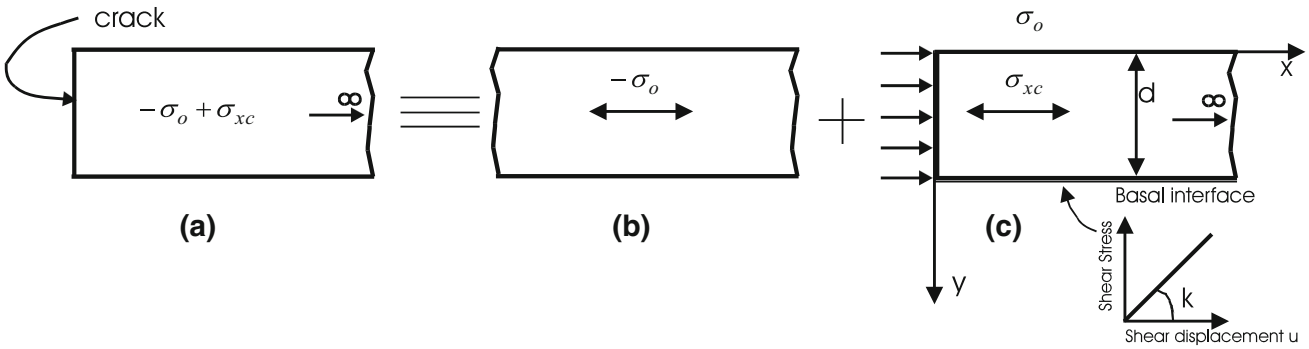

Fig. 1 Application of the superposition principle for computation of stress relief

horizontal compressive stress $\sigma_0(> 0)$ at the crack face. A solution for σ_x can be determined whether a solution for σ_{xc} is found. Compressive stresses are assumed to be positive.

The authors developed an approximate analytical solution for σ_{xc} (as shown in Fig. 1c) on the basis of an elastic stress analysis. (The details of the solution are given in Appendix to this paper.) Based on this analysis, the horizontal stress distribution on the top surface (i.e. $y = 0$) can be given by Eq. (2).

$$\frac{\sigma_{xc}^{y=0}}{\sigma_0} = e^{-\frac{1}{\sqrt{\frac{1}{(1-\nu)}+\frac{E}{kd(1-\nu^2)}}}\left(\frac{x}{d}\right)} \tag{2}$$

where E is elastic modulus, ν is the Poisson's ratio, k is the interface shear stiffness, and d is the depth of the layer. If plane stress conditions are assumed, the square root term in Eq. (2) will become $\sqrt{(1+\nu)+E/kd}$. The non-dimensional parameter, E/kd, signifies relative interface shear stiffness with respect to the top material surface. It is clear that the solution satisfies the boundary conditions; $\sigma_{xc} = \sigma_0$ when $x = 0$, and $\sigma_{xc}^{y=0} \rightarrow 0$ when $x \rightarrow \infty$.

Substituting Eq. (2) into (1) makes it possible to determine the horizontal tensile stress distribution ($\sigma_{xc}^{y=0}$) at the surface after the development of a crack:

$$\frac{\sigma_x^{y=0}}{(-\sigma_0)} = 1 - e^{-\frac{1}{\sqrt{\frac{1}{(1-\nu)}+\frac{E}{kd(1-\nu^2)}}}\left(\frac{x}{d}\right)} \tag{3}$$

The accuracy of this approximate solution was compared with a numerical solution obtained using a commercial finite difference numerical code, FLAC [15]. In the numerical simulation, an elastic layer of thickness d with basal interface as shown in Fig. 1c was used. A uniform horizontal stress of σ_{xc} was applied on the front vertical face. Figure 2a shows a comparison of the solution of Eq. (2) with the numerical solution for the condition of a fully restrained base signifying $E/kd = 0$. The solution is inaccurate close to the crack surface primarily because vertical equilibrium conditions are not satisfied in the analytical solution. However, the analytical solution

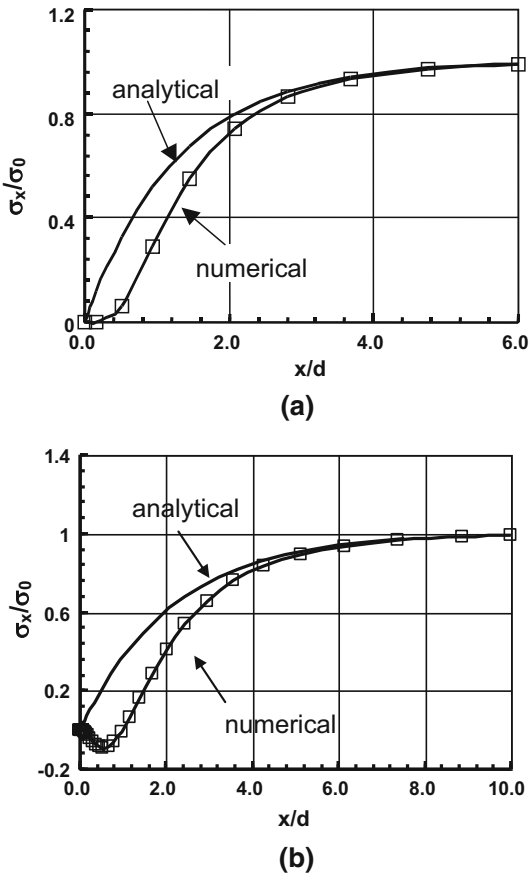

Fig. 2 Comparisons of numerical and analytical results for stress perturbation due to an isolated crack: **a** $\nu = 0.4$ and fixed base ($E/kd = 0$); **b** $\nu = 0.4$ and $E/kd = 3$

becomes reasonably accurate far away (at about $x = 3d$) from the crack surface and this is important for the prediction of crack spacing. As illustrated in Fig. 2b, similar observations can be made when nonzero E/kd values are applied at the bottom interface that undergoes elastic shear displacements immediately after cracking. Hence, it may be used to predict the approximate spacing of subsequent crack initiations by the stress relief approach.

3.1 Prediction of sequential crack spacing

Once the first crack occurs it may be assumed that $-\sigma_0 = -\sigma_t$, where σ_t (> 0) is the tensile strength of the material. Following the work of Konrad and Ayad [21] and Lachenbruch [22], it is assumed that a second crack would initiate when the horizontal tensile stress reaches $\alpha\,(\leq 1)$ times the tensile strength σ_t. If it is also assumed that this crack occurs reasonably fast and there is no change in tensile stress and tensile strength due to further drying, the following equation can then be derived from Eq. (3) for the non-dimensional crack spacing *s/d*, under plane strain conditions:

$$\left(\frac{s}{d}\right) = -\sqrt{\frac{1}{(1-v)} + \frac{E}{kd(1-v^2)}}\,\ln(1-\alpha) \tag{4}$$

An interesting practical feature of this equation is the fact that the crack spacing will increase for the same layer depth, as E/kd increases. For instance, the crack spacing may increase due to the interface getting more ductile (i.e. k reduces) or the material getting stiffer (E increases). For an ideally smooth surface (say, $E/kd \approx \infty$), cracks do not occur since the crack spacing become infinitely large. The crack spacing increases with layer depth when other variables are kept constant. These suggestions are compatible with general observations on cracking [9, 17].

4 Application of energy balance approach

Bazant and Cedolin [4] proposed an energy approach for the prediction of the spacing of shrinkage cracks formed during sudden cooling of hot rock media. It was postulated that the strain energy released during crack formation was balanced by the energy consumed during the formation of cracks. Under plane strain and isothermal conditions, the energy balance can be expressed by the following Eq. (4):

$$\int_V \Delta U\,\mathrm{d}V = G_c a \tag{5}$$

where ΔU is the strain energy released for a small soil element and V is the material volume which underwent strain release in association with a single crack. The parameter G_c is the crack energy release rate, which is related to material fracture toughness, K_{Ic}, under plane strain conditions by $K_{Ic} = \sqrt{G_c E/(1-v^2)}$, and a is the crack depth. Under linear elastic conditions, G_c is considered to be a material constant. This approach is applied to the simultaneous cracking of a desiccating layer in the following section.

4.1 Prediction of simultaneous crack spacing

It was assumed that cracks are formed simultaneously at a spacing s in an elastic soil layer of depth d that is placed on a hard surface as shown in Fig. 3. The energy balance can be taken into account by considering a single crack with vertical boundaries midway between adjacent cracks. The change in horizontal stress, ($\Delta\sigma_x$), due to crack formation can be expressed as:

$$\Delta\sigma_x = (-\sigma_0 + \sigma_{xc}) - (-\sigma_0) = \sigma_{xc} \tag{6}$$

Changes in other stress components $\Delta\sigma_y$ and $\Delta\tau_{xy}$ can also be established. Under plane strain conditions, the accompanying stress change in the z direction,$\Delta\sigma_z$, can be computed as $v(\Delta\sigma_x + \Delta\sigma_y)$. Therefore, the direct strain components $(\Delta\varepsilon_x, \Delta\varepsilon_y)$ and the shear strain component $(\Delta\gamma_{xy})$ associated with the crack formation can be computed using linear elastic stress–strain relations, involving Young's modulus E and Poisson's ratio v. The strain energy loss, ΔU, associated with this stress reduction can be computed by integrating the sum of average stress $\left(\sigma_x^{av}, \sigma_y^{av}, \tau_{xy}^{av}\right)$ times the respective strain component $(\Delta\varepsilon_x, \Delta\varepsilon_y, \Delta\gamma_{xy})$ over the area (i.e. unit length in z direction) influenced by a single crack as:

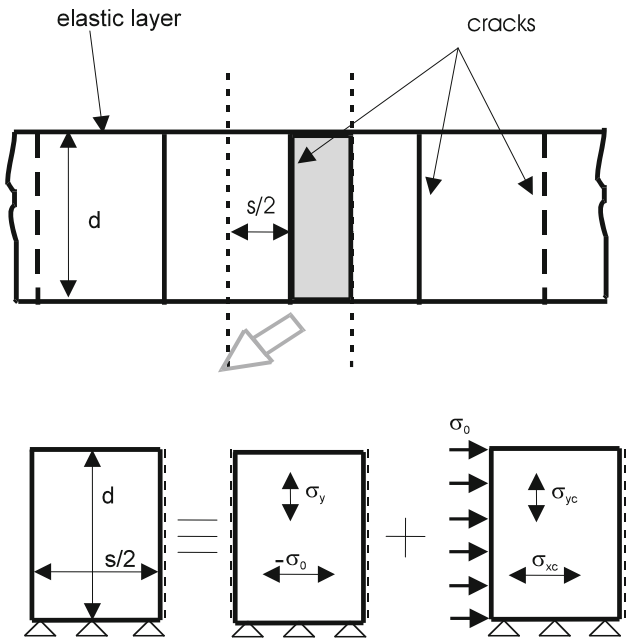

Fig. 3 Methodology used in the analysis of simultaneous cracking in an elastic layer with a fixed-hard base

$$\Delta U = \int_{-s/2}^{s/2} \int_{0}^{d} \left(\sigma_x^{\mathrm{av}} \Delta\varepsilon_x + \sigma_y^{\mathrm{av}} \Delta\varepsilon_y + \tau_{xy}^{\mathrm{av}} \Delta\gamma_{xy} \right) \mathrm{d}y\mathrm{d}x \tag{7}$$

Equation (7) can be expressed in a non-dimensional form as:

$$\Delta U^* = \frac{\Delta U E}{\sigma_o^2 d^2} = \int_{-s/2d}^{s/2d} \int_{0}^{1} \left(\left(\sigma_x^{\mathrm{av}} \Delta\varepsilon_x + \sigma_y^{\mathrm{av}} \Delta\varepsilon_y + \tau_{xy}^{\mathrm{av}} \Delta\gamma_{xy} \right) \frac{E}{\sigma_o^2} \right) d\left(\frac{y}{d}\right) d\left(\frac{x}{d}\right) \tag{8}$$

The non-dimensional strain energy loss, ΔU^*, was evaluated using the FLAC finite difference code. The same model developed earlier (with respect to Eq. 3) for stress relief approach was used here. The boundary conditions were chosen such that only a half of the area applicable to a single crack was modelled owing to symmetry about the crack plane (see Fig. 3). The strain energy associated with each element in the model was summed when evaluating the integral given in Eq. (7) using the numerical model. On the basis of an analytical formulation, it was established that ΔU^* was a function of the non-dimensional parameters *s/d* and *v*. Figure 4 shows the relationship of ΔU^* with *s/d* for $v = 0.4$ and $v = 0.3$. It is clear that the typical relationship of non-dimensional strain energy with *s/d* ratio (also the strain energy with spacing) has a similar shape to that of stress relief caused by an isolated crack. When *s/d* increases, ΔU^* asymptotically reaches a maximum value, $\Delta U^*_{\max}$. Based on the numerical model used, $\Delta U^*_{\max}$ appears to be unity. It is not completely clear why $\Delta U^*_{\max} = 1$ is obtained, but by expressing this condition as $\Delta U = 2\left(\frac{1}{2}\,\sigma_o\,\frac{\sigma_o}{E} d^2\right)$, it seems that the maximum strain energy that can be released by an isolated fully penetrating crack is equivalent to virtual release of full strain energy uniaxially up to a spacing of 2*d*. The influence of Poisson's ratio on the strain energy relationship appears to be less important. Based on the computations performed, ΔU^* tends to reach 99% of $\Delta U^*_{\max}$ around an *s/d* ratio of 10.

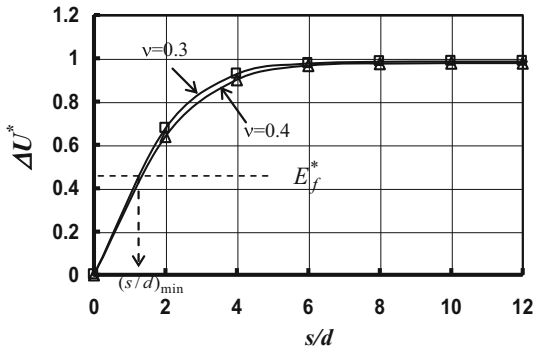

Fig. 4 Variation of non-dimensional strain energy (ΔU^*) with *s/d* ratio for simultaneous cracking

The energy balance during crack formation requires that ΔU must be balanced by energy consumed by the crack E_{f}, which is equal to $G_c d$ (per unit length in *z* direction). For fully penetrating cracks, however, there may be excess energy that is released in forms other than the crack surface energy. For example, this extra energy may lead to generation of heat, sound, plastic work or curved cracks. Therefore, using Eq. (8) and the same non-dimensionalisation procedure, the energy balance requirement may be expressed as:

$$\Delta U^* \geq E_{\mathrm{f}}^* \tag{9}$$

where $E_{\mathrm{f}}^* = \frac{G_c E}{\sigma_o^2 d}$, which is also given by $E_{\mathrm{f}}^* = \left(\frac{K_{\mathrm{Ic}}}{\sigma_o}\right)^2 \frac{(1-\nu^2)}{d}$. The requirement given by Eq. (9) is illustrated in Fig. 4, indicating that (*s/d*) ratio must be equal or greater than a certain minimum value, $(s/d)_{\min}$.

4.2 Prediction of sequential crack spacing

The energy balance approach can also be used to predict crack spacing if the cracks were to occur sequentially. In this case, the formation of the first crack will release stresses (and strain energy) in the soil layer in a manner similar to that considered in the stress relief approach. If shear displacements are allowed to occur at the basal interface, then further reduction in stresses could occur before the next crack initiates. It follows that the strain energy associated with the second (subsequent) crack formation is dependent on the characteristics of the basal interface. The modelling approach is illustrated in Fig. 5.

Figure 5a shows initial conditions with uniform horizontal stresses and a vertical gravity stress field contained by the horizontal restraints on either side of the soil layer. The spacing between the first and second cracks, crack width and the remaining length are marked by *s*, *e* and *l*, respectively. The length of the specimen is taken to be at least 20 times its thickness for it to be considered a thin, long layer. The basal interface is represented by a linear spring with shear stiffness *k*. Figure 5b shows the situation after the formation of the first crack at the left-hand boundary. When the *x* restraint is removed to simulate the first crack, some horizontal stresses are released. Interface shear displacements can also occur at the basal interface if the shear stiffness *k* is finite. Figure 5b also shows a typical schematic of the horizontal stress distribution at the surface after the stress release. As shown in Fig. 5c, the second crack is assumed to form at a spacing *s* from the first crack. This is modelled by forming a thin void in the elastic layer. The dimensional proportions used in the model are shown in Fig. 5. The strain energy loss associated with the formation of the second crack is computed as follows:

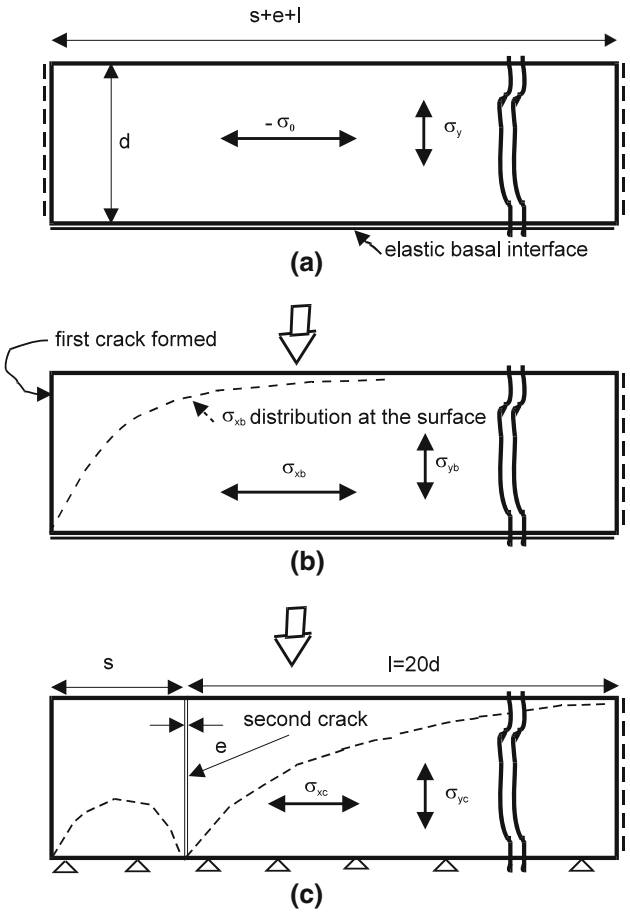

Fig. 5 Methodology used in the analysis of sequential cracking in an elastic layer with a hard base and elastic basal interface characteristics

$$\Delta U^* = \frac{\Delta UE}{\sigma_0^2 d^2} = \int_{-s/d}^{l/d} \int_0^1 \left(\left(\sigma_x^{\mathrm{av}} \Delta\varepsilon_x + \sigma_y^{\mathrm{av}} \Delta\varepsilon_y + \tau_{xy}^{\mathrm{av}} \Delta\gamma_{xy} \right) \frac{E}{\sigma_0^2} \right) d\left(\frac{y}{d}\right) d\left(\frac{x}{d}\right) \tag{10}$$

The stresses $(\sigma_x^{\mathrm{av}}, \sigma_y^{\mathrm{av}}, \tau_{xy}^{\mathrm{av}})$ in Eq. (10) correspond to the averages of the corresponding normal and shear stresses for conditions depicted in Fig. 5b and c, respectively.

The resulting ΔU^* relationships are functions of non-dimensional parameters, *s/d*, *ν*, *E/kd* and if gravity stresses are included, $\gamma d/\sigma_0$. However, in this instance, the general variation of ΔU^* is examined only for a range of *s/d* and *E/kd* parameters by using the FLAC computer program. Figure 6 shows typical results obtained. It should be noted that the same relationship between ΔU^*, and *s/d* is obtained for the condition of a fully restrained base (i.e. $E/kd = 0$), and for simultaneous cracking as shown in Fig. 4. As the *E/kd* parameter is reduced, the curves progressively flattened indicating that lower strain energy is available for subsequent crack formation at the same spacing. This reduction in strain energy loss is due to the increase in stress release

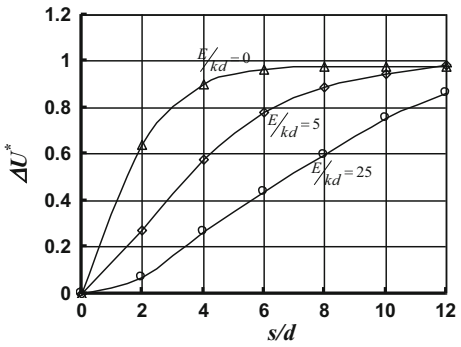

Fig. 6 Variation of non-dimensional strain energy (ΔU^*) with *s/d* ratio for sequential cracking ($\nu = 0.4$)

assisted by the ductile interface (i.e. low *k*). This feature can alternatively be viewed as the influence of the increased stress relief zone resulting from an increase in modulus or a decrease in layer thickness.

As for the simultaneous cracking, the formation of the subsequent (second) crack may be determined by balancing the energy released by the soil with the energy consumed during crack formation, (i.e. $\Delta U^* \geq E_f^*$). Therefore, a minimum spacing-to-depth ratio $(s/d)_{\min}$ can be found when there is an intersection between ΔU^* and E_f.

5 Minimum crack spacing

For fully restrained base condition (i.e. $E/kd = 0$), the variation of ΔU^* with *s/d* ratio is the same for both simultaneous cracking and sequential cracking (see Figs. 4, 6), and its dependence on Poisson's ratio is small. It is possible to represent this variation using an exponential curve as follows:

$$\Delta U^* = 1 - e^{-0.55\left(\frac{s}{d}\right)} \tag{11}$$

By using the non-dimensional energy balance at crack formation (i.e. $\Delta U^* \geq E_f^*$) and rearranging terms in the previous equation, the following equation is obtained.

$$\left(\frac{s}{d}\right)_{\min} = -1.82 \ln\left(1 - E_f^*\right) = -1.82 \ln\left(1 - \frac{G_c E}{\sigma_0^2 d}\right) = -1.82 \ln\left(1 - \left(\frac{K_{\mathrm{Ic}}}{\sigma_t}\right)^2 \frac{(1-\nu^2)}{d}\right) \tag{12}$$

At the rightmost part of Eq. (12), the condition, $-\sigma_o = -\sigma_t$ is assumed at the point of cracking rupture stress $(-\sigma_o)$ and is represented by the tensile strength of the material. It is interesting to compare Eq. (12) with (4), which was derived using the stress relief approach. On comparison, it could be argued that the arbitrary parameter

α used in Eq. (4) is related to the term, $(K_{Ic}/\sigma_t)^2(1-\nu^2)/d$. For the fully restraint base condition (i.e. $E/kd = 0$), the constant in Eq. (4) is equal to -1.3 and compares reasonably well with the constant -1.82 in Eq. (12). An exact match is not expected in any event because Eq. (4) is an approximate solution for stress relief. Nonetheless, it is clear that the energy balance and stress relief approaches are closely related, and the energy balance approach imposes a minimum spacing limit for cracks to occur. A normalisation of data presented in Fig. 6 gave the following approximation for ΔU^* and $(s/d)_{\min}$ for the general case:

$$\Delta U^* \approx 1 - e^{-\frac{0.66}{\sqrt{\frac{1}{(1-\nu)}+\frac{E}{kd(1-\nu^2)}}}\left(\frac{s}{d}\right)} \tag{13}$$

and

$$\left(\frac{s}{d}\right)_{\min} \approx -1.5\sqrt{\frac{1}{(1-\nu)}+\frac{E}{kd(1-\nu^2)}}\ln\left(1-\left(\frac{K_{Ic}}{\sigma_t}\right)^2\frac{(1-\nu^2)}{d}\right). \tag{14}$$

6 Critical layer thickness

Equation (12) [or (14)] also shows that $E_f^* = \left(\frac{K_{Ic}}{\sigma_t}\right)^2\frac{(1-\nu^2)}{d} < 1$ for a fully penetrating crack to occur under a uniform stress profile. This requirement can be rearranged to provide a critical layer thickness ($d_{\min}$) for cracking to occur.

$$d_{\min} = \left(\frac{K_{Ic}}{\sigma_t}\right)^2(1-\upsilon^2) \tag{15}$$

Equation (15) needs to be interpreted as the minimum thickness for fully penetrating cracking to occur in a thin layer of uniform suction. These conditions may not be satisfied when layer thickness is large under field conditions, but cracks may propagate progressively. For instance, several researchers [e.g. 8] have reported that drying of granular ceramic films with thicknesses ranging from tens to hundreds of micrometres has shown the presence of a similar critical layer thickness. This similarity can be explained using equations similar to Eq. (15). Figure 7 shows the variation of spacing-to-depth ratio with a normalised layer depth (given by $d\left(\sigma_t/K_{Ic}\right)^2$) computed using Eq. (14), for a range of *E/k* values. Also shown, in this figure is a fracture mechanics solution developed by Thouless [27] for brittle films on an elastic substrate with the same modulus. It should be noted that the present solution agrees reasonably well with this solution when no base slippage is allowed, (i.e. *E/k = 0)*. The figure also illustrates the presence of a critical layer thickness. Examination of Eq. (14) also shows that crack spacing decreases as the depth of the layer decreases, and cracks will disappear altogether at the critical depth.

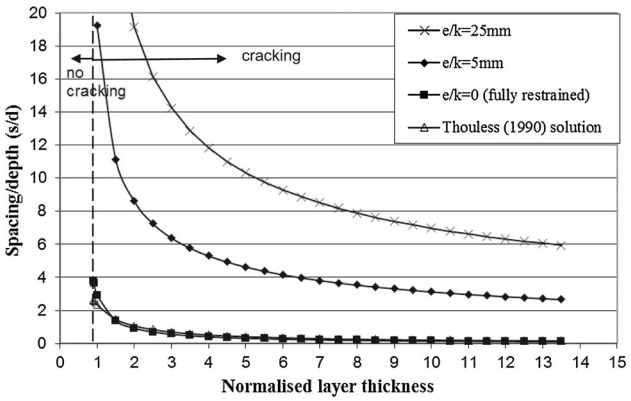

Fig. 7 Spacing/depth (s/d) ratio against normalised layer thickness given by $d\left(\sigma_t/K_{Ic}\right)^2$ (Poisson's ratio, $\nu = 0.4$)

7 Discussion and validation of the model using laboratory observations on soil desiccation cracking

The approximate theoretical development presented above is used to interpret observations on laboratory desiccation cracking tests. The test results are drawn from Corte and Higashi [9], who conducted tests in boxes with soil initially at slurry and loosely compacted states, and Nahlawi and Kodikara [23], who conducted cracking tests in long moulds conducive to parallel cracking with soil initially at slurry and compacted states.

7.1 Cracking water content, w_{cr}

Both Corte and Highashi [9] and Nahlawi and Kodikara [23] measured the soil water content at which cracking initiated. Some of their results are shown in Fig. 8. It is clear that the cracking water content decreases as the soil thickness is decreased. This requires a special explanation because according to the strength failure criterion, the failure stress should remain at the same cracking water content (assuming a unique soil–water characteristic curve) for the same initial conditions. Corte and Higashi [9] explained this observation assuming that the cracking water content was a function of desiccation rate (the desiccation rate increases with decreasing thickness, see [23]), where a high desiccation rate gives rise to less opportunity for micro-crack coalescence. An alternative explanation is now proposed on the basis of a critical layer thickness.

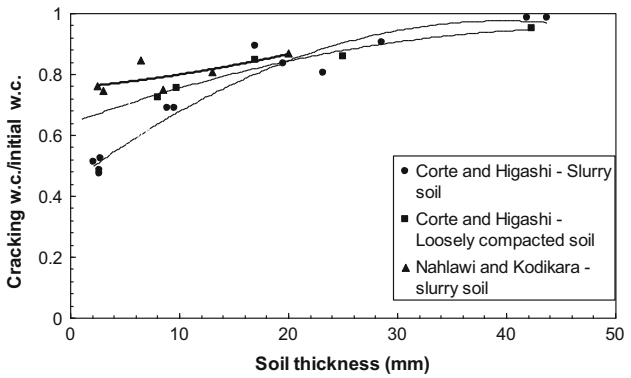

Fig. 8 Cracking water content normalised by initial water content against soil thickness

According to Eq. (15), if the soil thickness is less than the corresponding critical thickness, then cracks will not occur. If this is the case, the soil will need to dry further in order that the critical thickness, which is a function of $(K_{Ic}/\sigma_t)^2$, can decrease sufficiently to allow cracking to occur. There is experimental evidence that $(K_{Ic}/\sigma_t)^2$ decreases as the material becomes brittle. For instance, Haberfield and Johnston [13] indicated that this term can take values of 9 mm for harder rocks, 11 mm for relatively soft mudstones and as much as 466 mm for soft clays. Ayad et al. [3] reported some results for soft marine silty clay which gave a value of about 20 mm for $(K_{Ic}/\sigma_t)^2$. Experimental data presented by Wang et al. [29] also confirm the decreasing trend of $(K_{Ic}/\sigma_t)^2$ during drying. Values calculated from their results show that this ratio reduces from 125 to 107 mm as the dry density increases from 1.6 to 1.72 g/cm^3 (during drying dry density increases as soil shrinks, see [25]). Therefore, for clay soils, this ratio can decrease as the soil dries. A comprehensive data set would be useful for a closer examination of this issue.

A decreasing cracking water content is also apparent when the desiccation rate (rate of decrease in water content with time) is increased [9, 11, 23]. It is apparent that as the layer thickness is decreased, the desiccation rate increases, explaining this dependency. For thicker layers, Costa et al. [11] suggested the existence of an effective drying depth (i.e. the depth of tensile stress profile, which could be sharply curved) which can be captured by the ratio between soil moisture diffusivity and evaporation rate. Effective depth becomes small under high desiccation rates. When an effective depth exists in a thick soil layer subjected to desiccation, the situation will be similar to having a layer with a smaller thickness despite the overall layer thickness being relatively large.

7.2 Crack spacing/layer depth ratio, (*s/d*)

Figure 9 shows a comparison of mean (*s/d*) ratios with depth between theoretical and experimental results of Nahlawi and Kodikara [23] for compacted and slurry soils. Nahlawi and Kodikara [23] identified three forms of cracking, namely primary, secondary and tertiary cracking in experimental observations on parallel cracking when drying long soil layers. Primary cracking was defined as when the first set of cracks appear, while secondary cracks occur between two primary cracks. Tertiary cracks were defined as those cracks that occur between a primary crack and a secondary crack or between other crack combinations. In the current analysis, sequential cracking strictly refers to primary cracking that occurs in sequence. In other words, only one crack influences the formation of the next crack. The results relevant to primary cracks are presented in Fig. 9. It is clear that the (*s/d*) ratio decreases with layer depth, and this behaviour is generally captured by the model. However, layers with smaller depths (i.e. close to the critical depth) show a sharper decrease in the (*s/d*) ratio. In reality, the parameters $(K_{Ic}/\sigma_t)^2$ and *E/k* vary as the cracking water content changes for different layer depths, limiting the precise application of the model.

7.3 Evolution of cracking patterns

When the normalised fracture energy required for cracking is small (i.e. $E_f^* << 1$; refer Fig. 4), the non-dimensional fracture energy will intersect the ΔU^* curve at a relatively low *s/d* ratio, giving a small $(s/d)_{min}$. This means that there is sufficient energy to generate a full crack at a spacing greater than $(s/d)_{min}$. The strain energy available per unit volume of soil for crack propagation can become very large for small *s/d* ratios [for instance, from Eq. [8], strain energy per unit volume, $(\Delta U/sd) = \Delta U^*\left(\sigma_o^2/E(s/d)\right)$, which will increase (*s/d*) decreases]. At these levels, cracks need to release relatively large amounts of strain energy per

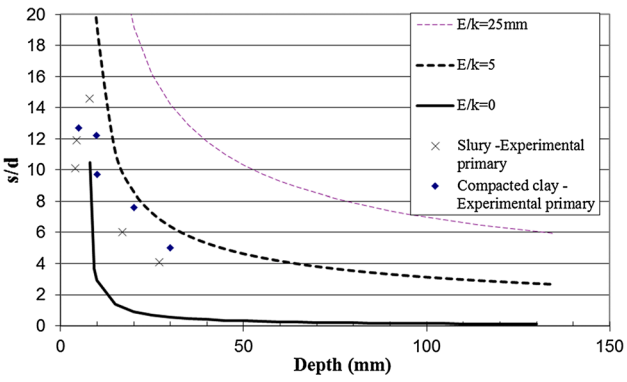

Fig. 9 A comparison of theory and experimental results of Nahlawi and Kodikara (2006) for (s/d) ratio with depth

unit volume of soil. Consequently, simultaneous cracking appears to be the optimal mechanism at relatively small spacing. Alternatively, cracks can still occur at larger sequential spacing because the energy balance requires that *s/d* to be only greater than $(s/d)_{\min}$. Lower E_f^* is likely to be generated for materials with a lower $(K_{Ic}/\sigma_t)^2$ ratio, which is associated with brittle materials with lower water contents, or with very loose soil deposits.

When E_f^* is close to unity, theoretically, sequential and simultaneous cracking are equally possible. However, it would appear that sequential cracking is more likely to dominate because these cracks can be triggered by a small local variation of parameters such as the tensile strength of the soil (or larger flows). The field studies [3, 22] have indicated that E_f^* [or α in Eq. (4)] can be over 80% for sequential crack formation. The actual *s/d* ratio of the cracking will be dependent on the local variation of tensile strength, and E_f^* will only impose the minimum requirement of (*s/d*) ratio possible. The other point is that during sequential cracking, the influence of ductility (given by *E/kd*) can come into play (see Fig. 6) causing this form of cracking to be more favoured. Soft ductile materials like soft clay feature a higher (K_{Ic}/σ_t) ratio giving a higher E_f^* and higher interface ductility and, therefore, are more likely to fail by sequential cracking. These theoretical inferences are in agreement with generally observed behaviour.

8 Concluding remarks

Theoretical explanations were provided for desiccation cracking of thin elastic soil layers subjected to a uniform stress (suction) profile. The spacing-to-depth ratio of fully penetrating cracks was analysed on the basis of both a stress relief and a fracture energy balance approach. It was shown that the energy required for crack formation places a lower limit for the spacing-to-depth ratio. In agreement with experimental observations, it was shown that the spacing-to-depth ratio decreases with layer depth. However, theory showed that there exists a critical depth of the layer below which cracking may not occur or the spacing-to-depth ratio is infinite. Similar arguments have been put forward with respect to the drying of thin ceramic films where defect-free films were impossible to manufacture above the critical depth. The influence of the stiffness at the base interface was also analysed. In agreement with experimental observations, it is clear that decreasing the basal interface stiffness makes the crack spacing increase for sequential crack formation where the final limit is that no cracks will appear if the basal interface is perfectly smooth. The experimental observation of a decrease in cracking water content with a decrease in layer thickness was also explained on the basis of the critical depth concepts. From a practical standpoint, this issue is only relevant for very thin soil layers.

The theoretical explanations were consistent with some experimental observations, but it should be noted that a number of simplifying assumptions were made. The main assumption involves the neglect of a change in the tensile stress profile, material properties and behaviour with time during desiccation. In future studies, it would be enlightening to examine these issues from both an experimental and theoretical approach.

Appendix

Approximate analytical solution for horizontal stress relief due to an isolated crack in an elastic layer with a hard base.

A solution is presented for a horizontal stress σ_{xc} for the situation depicted in Fig. 1c. The governing equations can be described as follows. The sign convention uses compressive stress as positive and clockwise shear as positive. This is traditional in soil mechanics. For horizontal equilibrium,

$$\frac{\partial \sigma_{xc}}{\partial x} = -\frac{\partial \tau_{xy}}{\partial y} \tag{16}$$

where τ_{xy} is the shear stress in *xy* plane. Ignoring normal stress change in *y* direction and considering plane strain condition, σ_{xc} can be expressed as:

$$\sigma_{xc} = -\frac{E}{(1-v^2)}\frac{\partial u}{\partial x} \tag{17}$$

where *u* is the shear displacement in *x* direction. *E* and *v* are the Young's modulus and Poisson's ratio of the soil, respectively. The shear stress is assumed to follow a linear stress distribution as follows:

$$\tau_{xy} = \left(\frac{y}{d}\right)\tau_b \tag{18}$$

where τ_b is the shear stress at the basal interface. Assuming a spring of shear stiffness of *k* to represent the basal interface characteristics, τ_b can be related to the shear displacement at the base u_b as:

$$\tau_b = k u_b \tag{19}$$

Ignoring the shear strain component associated with vertical displacement, the shear stress τ_{xy} can be expressed:

$$\tau_{xy} = -G\frac{\partial u}{\partial y} \tag{20}$$

Equations (16), (18) and (19) can be rearranged to give:

$$\frac{\partial^2 \sigma_{xc}}{\partial x^2} = -\frac{k}{d}\frac{\partial u_b}{\partial x} \tag{21}$$

Also, Eqs. (18), (19) and (20) can be rearranged to obtain:

$$\frac{\partial u}{\partial y} = -\frac{k}{G} u_b \frac{y}{d} \tag{22}$$

Equation (22) can be solved for u by using the boundary condition $u = u_b$, $y = d$. Using this result and Eq. (17), it is possible to obtain the following expression from Eq. (21).

$$\frac{\partial^2 \sigma_{xc}}{\partial x^2} - \frac{1}{d^2} \frac{1}{\left[\frac{1}{(1-\nu)} + \frac{E}{kd}\frac{1}{(1-\nu^2)}\right]} \sigma_{xc} = 0 \tag{23}$$

Equation (23) can be solved subject to the boundary conditions: $\sigma_{xc} = \sigma_0$ when $x = 0$; and $\sigma_{xc} \to 0$ when $x \to \infty$. The solution for $\sigma_{xc}^{y=0}$ in non-dimensional form can be expressed as:

$$\frac{\sigma_{xc}^{y=0}}{\sigma_0} = e^{-\frac{1}{\sqrt{\frac{1}{(1-\nu)} + \frac{E}{kd}\frac{1}{(1-\nu^2)}}}\left(\frac{x}{d}\right)}. \tag{24}$$

References

1. Amarasiri AL, Kodikara JK (2013) Numerical modelling of a field desiccation test. Geotechnique 63(11):983–986
2. Amarasiri AL, Kodikara JK, Costa S (2011) Numerical modelling of desiccation cracking. Int J Numer Anal Methods Geomech 35:82–96
3. Ayad R, Konrad R-M, Soulié M (1997) Desiccation of sensitive clay: application of the model CRACK. Can Geotech J 34:943–951
4. Bazant PZ, Cedolin L (1991) Stability of structures. Oxford University Press, Oxford
5. Chertkov VY, Ravina I (1998) Modelling the crack network of swelling clay soils. Soil Sci Soc Am J 62:1162–1171
6. Chertkov VY, Ravina I (1999) Morphology of horizontal cracks in swelling soils. Theor Appl Fract Mech 31:19–29
7. Chertkov VY, Ravina I (2004) Networks originating from the multiple cracking of different scales in rocks and swelling soils. Int J Fract 128:263–270
8. Chiu RC, Garino TJ, Cima MJ (1993) Drying of granular ceramic films: I effect of processing variables on cracking behaviour. J Am Ceram Soc 76(9):2257–2264
9. Corte A, Higashi A (1960) Experimental research on desiccation cracks in soil. Research Report, U. S. Army Snow Ice and Permafrost Research Establishment Research Report No. 66, Corps of Engineers. Wilmette, Illinois, USA
10. Costa S, Htike WY, Kodikara J, Xue J (2016) Determination of *J*-integral for clay during desiccation. Environmental Geotechnics EG6:372-378
11. Costa S, Kodikara J, Shannon B (2013) Salient factors controlling desiccation cracking of clay in laboratory experiments. Geotechnique 63(1):18–29
12. Gui YL, Zhao ZY, Kodikara J, Bui HH, Yang SQ (2016) Numerical modelling of laboratory soil desiccation cracking using UDEC with a mix-mode cohesive fracture model. Eng Geol 202:14–23
13. Haberfield CM, Johnston IW (1989) Relationship between fracture toughness and tensile strength for geomaterials. In: Proceedings of the 12th international conference on soil mechanics and foundation engineering, Rio de Janeiro, A.A. Balkema, 1:47–52
14. Huang M, Bruch PG, Barbour SL (2013) Evaporation and water redistribution in layered unsaturated soil profiles. Vadose Zone J 12(1). https://doi.org/10.2136/vzj2012.0108
15. Itasca Consulting Group (1993) FLAC, Fast Lagrangian Analysis of Continua. Ver: 3.2, Minnesota, USA
16. Kindle EM (1917) Some factors affecting the development of mud cracks. J Geol 25:135–144
17. Kodikara JK, Barbour SL, Fredlund DG (2000) Desiccation cracking of soil layers. In: Proceedings of asian conference on unsaturated soils: from theory to practice. Edited by Rahardjo H, Toll DG, Leong EC, A.A. Balkema 693–698
18. Kodikara JK, Barbour SL, Fredlund DG (2002) Structure development in surficial heavy clay soils: a synthesis of mechanisms. Aust Geomech 37(3):25–40
19. Kodikara JK, Choi X (2006) A simplified analytical model for desiccation cracking of clay layers in laboratory tests. In: Proceedings of UNSAT 2006 conference. Edited by Miller GA, Zapata CE, Houston SL, Fredlund DG. ASCE Geotechnical Special Publication, Unsaturated Soils, 2:2558–2567
20. Kodikara JK, Nahlawi H, Bouazza A (2004) Modelling of curling in desiccating clay. Can Geotech J 41:560–566
21. Konrad J-M, Ayad R (1997) An idealized framework for the analysis of cohesive soils undergoing desiccation. Can Geotech J 34:477–488
22. Lachenbruch AH (1961) Depth and spacing of tension cracks. J Geophys Res 66(12):4273–4292
23. Nahlawi H, Kodikara JK (2006) Laboratory experiments on desiccation cracking of thin soil layers. J Geotech Geol Eng 24:1641–1664
24. Peron H, Hueckel T, Laloui L, Hu LB (2009) Fundamentals of desiccation cracking of fine-grained soils: experimental characterization and mechanisms identification. Can Geotech J 46:1177–1201
25. Sanchez M, Atique A, Kim S, Romero E, Zielinski M (2013) Exploring desiccation cracks in soils using a 2D profile laser device. Acta Geotech 8:583–596
26. Shin H, Santamarina JC (2011) Desiccation cracks in saturated fine-grained soils: particle-level phenomena and effective-stress analysis. Geotechnique 61(8):961–972
27. Thouless MD (1990) Crack spacing in brittle films on elastic substrates. J Am Ceram Soc 73(7):2144–2146
28. Vo TD, Pouya A, Hemmati S, Tang AM (2017) Numerical modelling of desiccation cracking of clayey soil using a cohesive fracture method. Comput Geotech 85:15–27
29. Wang JJ, Zhu JG, Chiu CF, Zhang H (2007) Experimental study on fracture toughness and tensile strength of a clay. Eng Geol 94:65–75
30. White EM (1986) Longevity and effect of tillage-formed soil surface cracks on water infiltration. J Soil Water Conserv 41(5):344–347